Structural and mechanistic insights on a Fe^{3+}-triggered quinazoline based molecular rotor

Rampal Pandey,[a,b] Gábor Méhes,[c] Amit Kumar,[a] Rakesh Kumar Gupta,[a] Chihaya Adachi[c,d] and Daya Shankar Pandey*[a]

[a]Department of Chemistry, Faculty of Science, Banaras Hindu University, Varanasi-221005, India

[b]Department of Chemistry, Dr. Hari Singh Gour University, Sagar-470003 (M. P.,) India

[c]Department of Applied Chemistry, Center for Organic Photonics and Electronics Research (OPERA), Kyushu University, 744 Motooka, Nishi, Fukuoka 819-0395, Japan.

[d]International Institute for Carbon Neutral Energy Research (WPI-I2CNER), Kyushu University, 744 Motooka, Nishi, Fukuoka 819-0395, Japan.

Contents:

1. Materials and methods

The solvents were dried and distilled following standard literature procedures prior to their use.[1] Metal nitrates viz., $NaNO_3$, KNO_3, $Ca(NO_3)_2{\cdot}4H_2O$, $Mg(NO_3)_2{\cdot}6H_2O$, $Fe(NO_3)_3{\cdot}9H_2O$, $FeCl_2{\cdot}4H_2O$, $FeCl_3{\cdot}6H_2O$, $Co(NO_3)_2{\cdot}6H_2O$, $Ni(NO_3)_2{\cdot}6H_2O$, $Cu(NO_3)_2{\cdot}3H_2O$, $Zn(NO_3)_2{\cdot}6H_2O$, $Cd(NO_3)_2{\cdot}4H_2O$, $AgNO_3$, $Pb(NO_3)_2$, $Hg(NO_3)_2$ and 2,6-diacetylpyridine, 2-acetylpyridine and 2-aminophenylbenzimidazole were procured from commercial sources and used without further purifications.

1.1 Synthesis

Synthesis of 6-methyl-6-pyridin-2-yl-5,6-dihydro-benzo[4,5]-imidazo[1,2c]quinazoline (1): 2,6-diacetylpyridine (3.0 mmol) was added to a stirring solution of 2-(2-aminophenyl)-1-benzimidazole (6.0 mmol) in ethanol (25 mL) and the resulting reaction mixture heated under reflux for 8 h. After cooling to ambient temperature it was concentrated at reduced pressure to half its volume and kept undisturbed in a refrigerator. The microcrystalline compound thus obtained was separated by filtration, washed with cold ethanol followed by diethyl ether and re-crystallized using methanol. Yield (**1**, 0.502 g, 92.1%): mp 218-220 ºC. Analytical data: Anal. Calc. for $C_{35}H_{27}N_7$ (545.23): C, 77.04; H, 4.99; N, 17.97. Found: C, 77.09; H, 4.99; N, 18.01. FT-IR (KBr; cm^{-1}): 3359 (m), 1612 (m), 1587 (m), 1539 (s), 1478 (s), 1375 (m), 1309 (m), 753 (vs), 733 (vs). ^{1}H NMR (DMSO-d_6, 300 MHz, δ_H, ppm): 7.88 [d (*br*), H7, 2*H*]; 7.52-7.62 (m, H-4, H-8, 4*H*); 7.44 (s, H-1, 2H, N*H*); 7.32-7.13 (m, H-5, H-6, H-2, 6*H*); 6.91□6.80 (m, H-3, H-9, H-10, H-11, 7*H*); 2.12 (s, H-12, 3H); 2.05 (s, H-12, 3H). ^{13}C NMR (DMSO-d_6, 75 MHz, δ_C, ppm): 159.87, 147.29, 142.87, 138.94, 133.23, 131.54, 124.64, 121.89, 120.22, 118.67, 114.42, 111.80, 25.72. HRMS (*m/z*) for $C_{35}H_{27}N_7$: [M+H$^+$] calcd 545.2328; found 546.2323.

Synthesis of 6-methyl-6-pyridin-2-yl-5,6-dihydro-benzo[4,5]-imidazo[1,2-c]quinazoline hydrochloride·2H$_2$O (1'): An aqueous solution (2 mL) of $FeCl_3{\cdot}6H_2O$ (0.269 g, 1.0 mmol) was added drop wise to a solution of **1** (0.545 g, 1.0 mmol) in methanol (10 mL) and resulting reaction mixture stirred for 10 minutes. A light green colored product appeared quickly which was filtered, washed thrice with water (3×5 mL), to remove free iron metal from the reaction mixture. The resulting greenish colored residue was re-crystallized from methanol to afford **1′**. Yield (0.588 g, 90%). Analytical data: Anal. Calc. for $C_{35}H_{33}Cl_2N_7O_2$ (654.58); C, 64.22; H,

5.08; N, 14.98. Found: C, 64.28; H, 5.12; N, 15.04%. FT-IR (KBr; cm^{-1}): 3517 (s), 3426 (m), 3260 (s), 1627 (vs), 1568 (s), 1458 (m), 1385 (s), 1185 (s), 754 (vs), 741 (vs). ^{1}H NMR (DMSO-d_6, 300 MHz, δ_H, ppm): 8.20 [s (*br*) H-1, 2H, □*NH*] 8.02-7.96 (m, H-4, H-7, 4*H*); 7.79-7.70 (m, H-5, H-6, 4H); 7.38 (d, J = 6.6 Hz, H-8, H-11, 4H); 7.08 [s (*br*), H-2, 2H]; 6.88 (m, H-3, H-9, H-10, 5H); 2.18 (s, H-12, 3H); 2.11 (s, H-12, 3H). ^{13}C NMR (DMSO-d_6, 75 MHz, δ_C, ppm): 158.01, 145.02, 143.67, 139.96, 135.28, 129.93, 125.39, 121.40, 118.62, 114.63, 112.94, 25.22. HRMS (*m/z*) for $C_{35}H_{33}Cl_2N_7O_2$: [M^+] calcd. 654.2106; found 654.1609.

2. General Methods.

Elemental analyses for C, H and N were performed on an Exeter Analytical Inc. Model CE-440 CHN analyzer. IR spectra were acquired on a Perkin-Elmer 577 spectrometer. ^{1}H (300 MHz) and ^{13}C (75.45 MHz) NMR spectra were obtained on a JEOL AL300 FT-NMR spectrometer using tetramethylsilane ($Si(CH_3)_4$) as an internal reference. Electronic absorption spectra were acquired on JASCO V-670 and Lambda 950, PerkinElmer spectrophotometers. Fluorescence spectra at rt were recorded on a PerkinElmer *LS 55* and Fluoromax 4, Horiba Fluorescence spectrophotometers. Photoluminescent quantum yield for all the samples and PL emission spectra on powder samples were measured using an absolute PL quantum yield spectrometer (C11347 Quantaurus QY, Hamamatsu), which incorporated an integrating sphere and a xenon lamp for excitation through a monochromator. The transient PL characteristics of all the samples and PL emission spectra on films were measured using a fluorescence lifetime spectrometer (C11367-12, Quantaurus-Tau, Hamamatsu), with embedded LED light source. The decay constants and fitting parameters (τ_1,τ_2, A_1, A_2) for transient decays were determined using the embedded software of Quantaurus-Tau. Mass spectra for **1** and **1´** were recorded on a JEOL-AccuTOF JMS-T100 LC Mass spectrometer using methanol as a solvent.

3. X-ray structure determinations.

Single crystal X-ray data for **1** and **M** were collected on Bruker APEX II (kappa 4) diffractometer and for **1'** on a OXFORD DIFFRACTION X CALIBUR-S at 25°C using graphite monochromatized Mo-Kα radiation (λ = 0.71073 Å). Structures were solved by direct methods (SHELXS 97) and refined by full-matrix least squares on F^2 (SHELX 97).[2] The non-hydrogen atoms were refined with anisotropic thermal parameters. All the hydrogen atoms were geometrically fixed and refined using a riding model. Computer program PLATON was used for

analyzing the interaction and stacking distances.[3] CCDC deposition numbers 959911 (**1**), 959912 (**1´**) and 959913 (**M)** contain supplementary crystallographic data for this paper.

4. UV/VIS and Photoluminescence (PL) studies.

Stock solution of **1** for electronic absorption and emission studies was prepared in H_2O/MeOH (1:1, v/v; *c*, 10 μM), and for various metal ions (Li^+, Na^+, K^+, Mg^{2+}, Ca^{2+}, Fe^{2+}, Fe^{3+}, Co^{2+}, Ni^{2+}, Cu^{2+}, Zn^{2+}, Cd^{2+}, Hg^{2+}, Ag^+, and Pb^{2+}) by dissolving their nitrate salts in triple distilled water (10 mM). In the titration experiments, 2.0 mL solution of **1** (10 μM) was taken in a quartz cuvette (3 mL, path length, 1 cm) and solution of the Fe^{3+} ion ($FeCl_3$) was added gradually with the help of a micro-pipette. In titration experiments the addition time interval for each fraction of the metal ion (Fe^{3+}) was 2 minute.

Thin films were fabricated on 1 mm thick quartz substrates by spin coating in a glove box with concentration of water and oxygen < 1 ppm. Before film fabrication the substrates were cleaned with chloroform and acetone in an ultrasonic bath. The compounds **1** (3.1 mg) and **1'** (3.3 mg) were dissolved in 1 ml of methanol and stirred for ca. 20 minutes in glove box. Spin rates were 3000 rpm for 30 seconds for each.

5. Electrochemical studies.

Stock solution of **1** for cyclic voltammery was prepared in H_2O/MeOH (1:1, v/v; *c*, 100 μM) using 0.1 M KCl as supporting electrolyte in the potential range of + 8.0 to - 0.8 V at rt. For Fe^{3+} ion (0.1 M), by dissolving its chloride salt ($FeCl_3$) in triple distilled water. In titration experiments the addition time interval for each fraction of the metal ion (Fe^{3+}) was 2 minute.

6. Calculation of energies

Following procedure was adopted to calculate the energetic properties of **1** and **1´**. 2D molecular structure of the molecules were designed using ChemBioDraw Ultra software and 3D structure was optimized using the same software by minimizing energy of the molecule using *MM2* mode. Resulting structure was further optimized using Gaussian 09 by performing a density functional theory (DFT) calculation in the B3LYP mode with a 6-31G(d) basis set in the ground state. These results were used to obtain highest occupied molecular orbital (HOMO) and lowest unoccupied molecular orbital (LUMO) levels and electron density distributions on these levels. The energetic properties of **1** and **1'** in excited state (singlet and triplet energy levels)

were determined using Gaussian 09 with the same basis set, but in time dependent mode (TD-DFT). To obtain the singlet and triplet energy levels with greater precision number of states was set to 10. Ground state dipole moments were part of the log-file of the above described DFT calculation, and excited state dipole moments were obtained in TD-DFT with additional ommand "density=current pop=chelpg" and selecting the state of interest according to S_1 or T_1 levels.

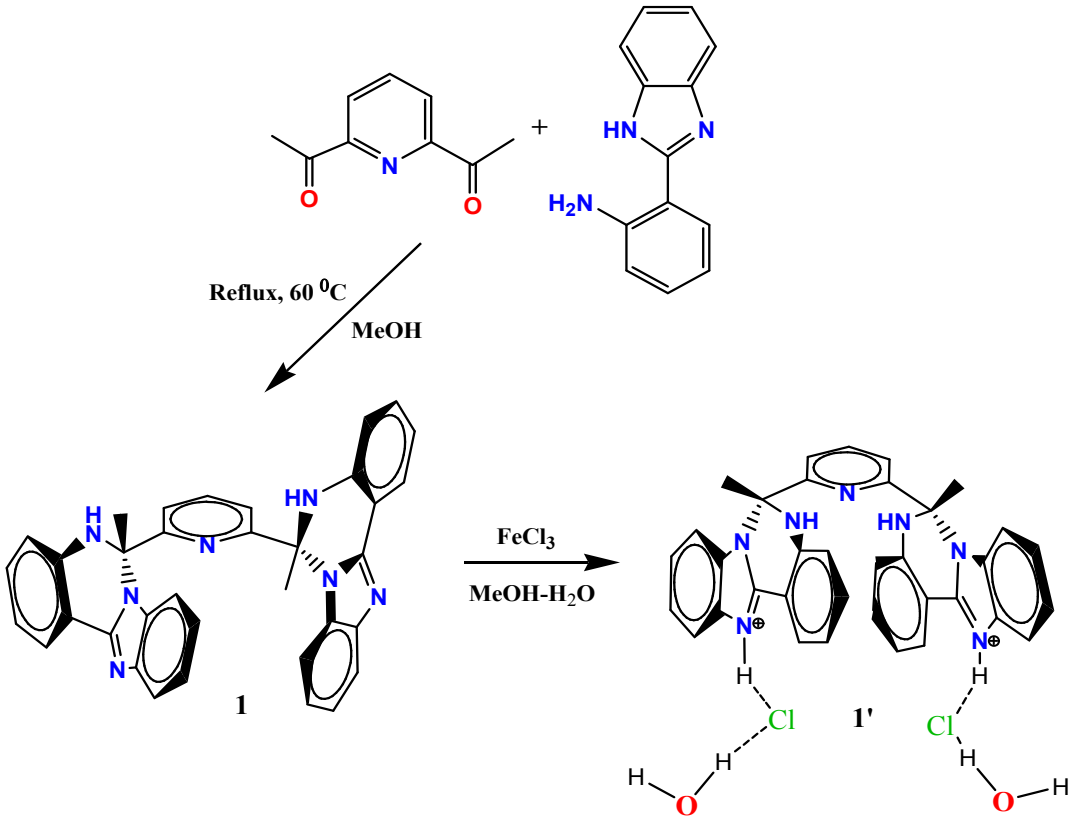

Scheme S1. Synthesis of compounds **1** and **1′**.

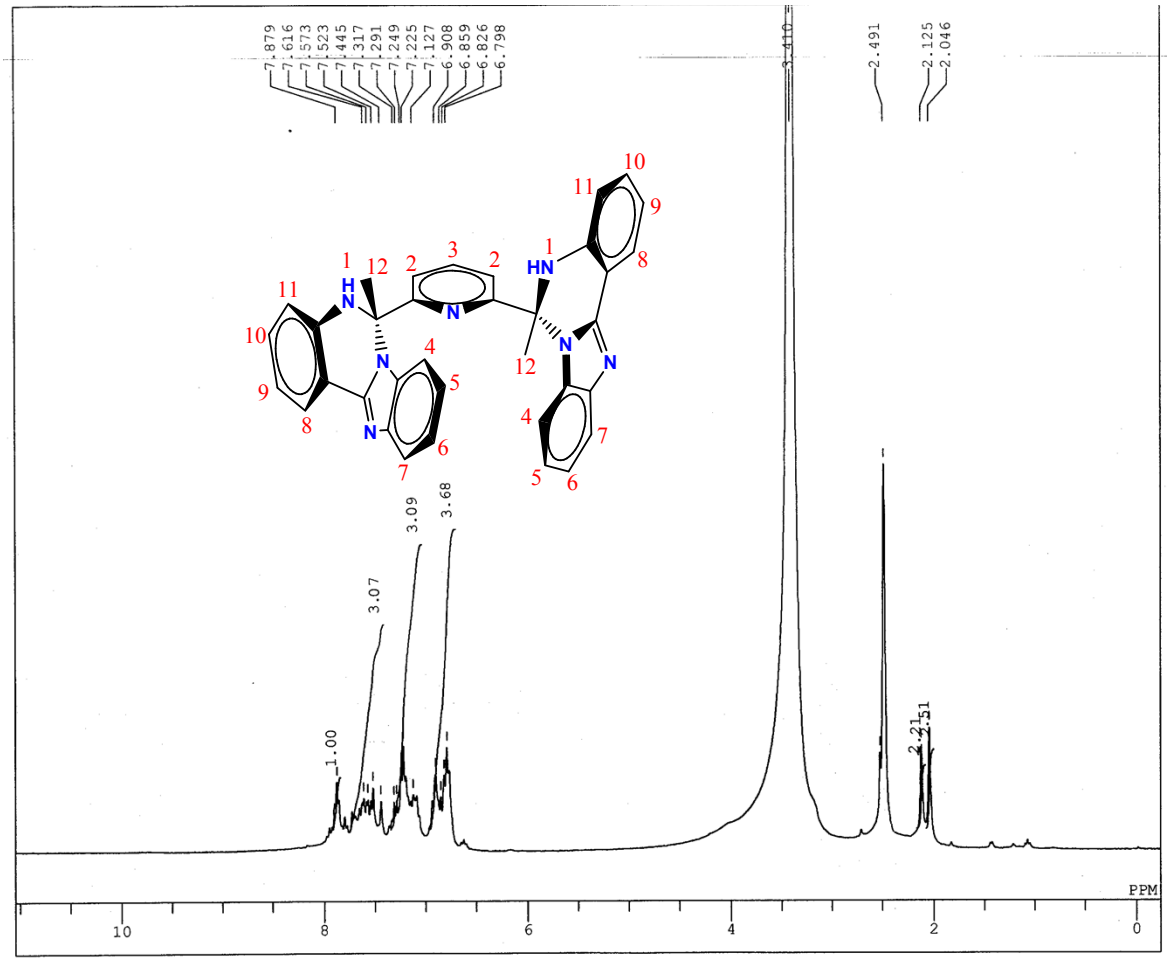

Fig. S1a ^{1}H NMR spectrum of **1** in dmso-d_6

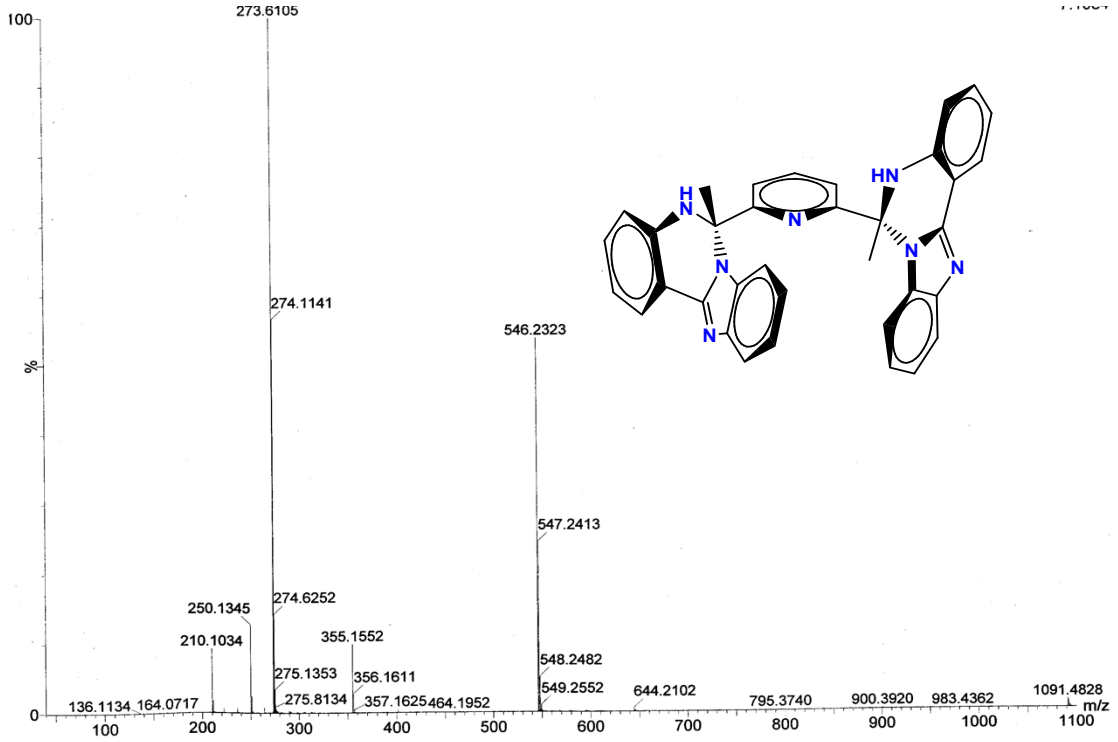

Fig. S1b HRMS spectrum of **1**

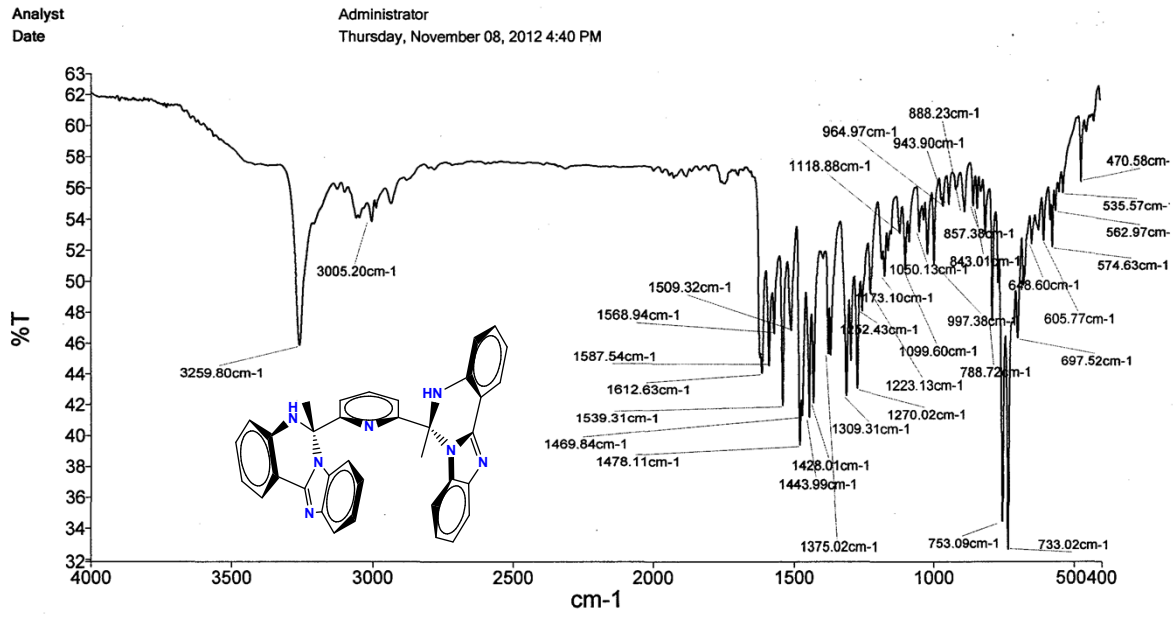

Fig. S1c IR spectrum of **1**

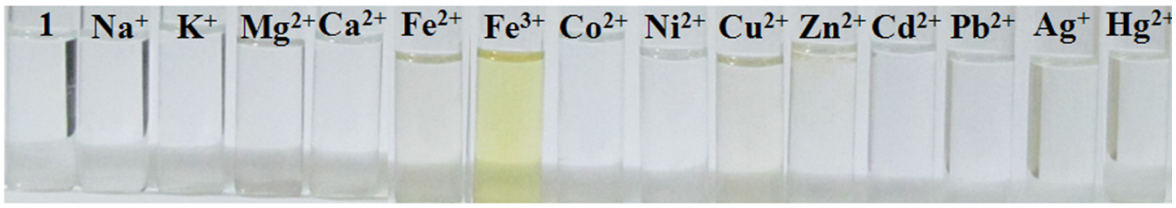

Fig. 2 Chromogenic response of **1** toward 2.0 equiv of various metal ions

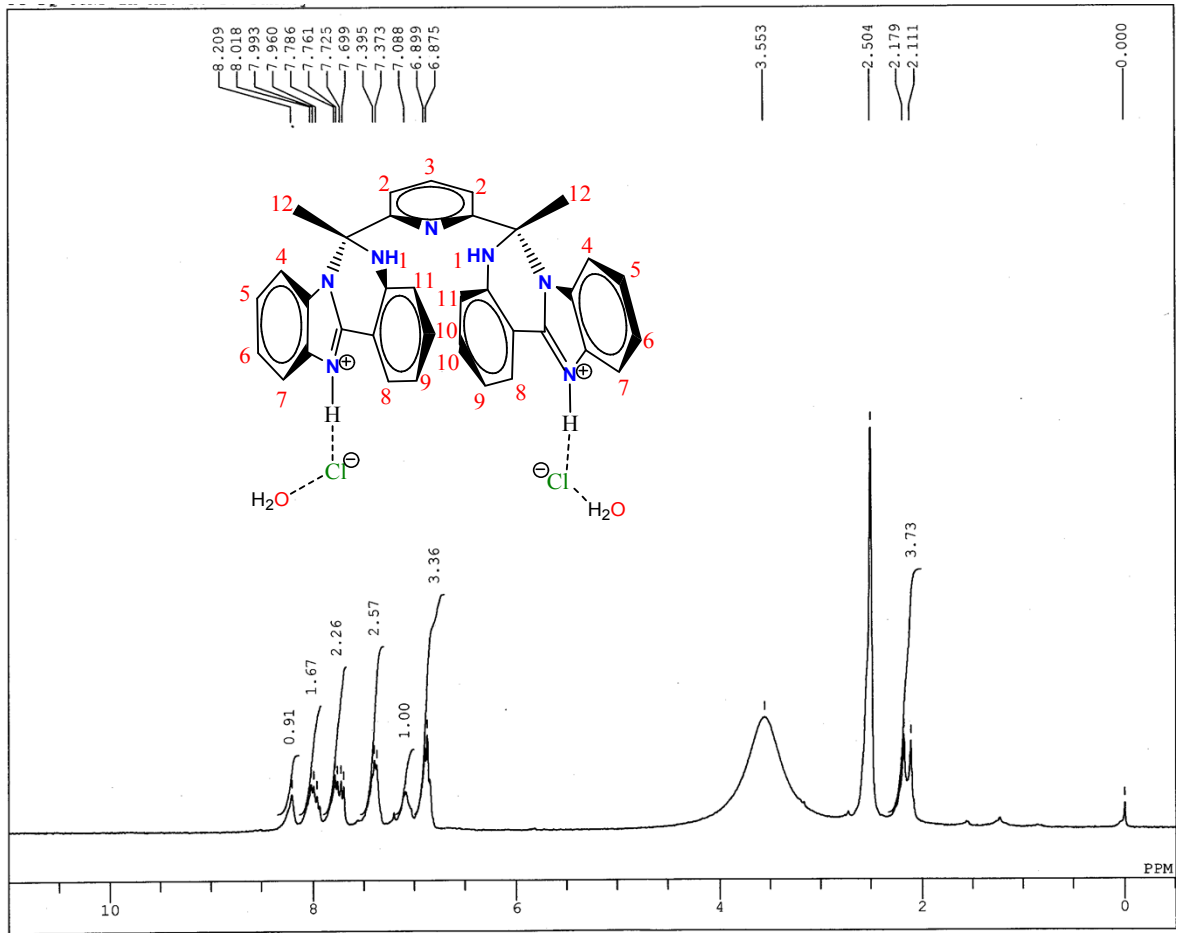

Fig. S3 ^{1}H NMR spectrum of **1′** in dmso-d_6

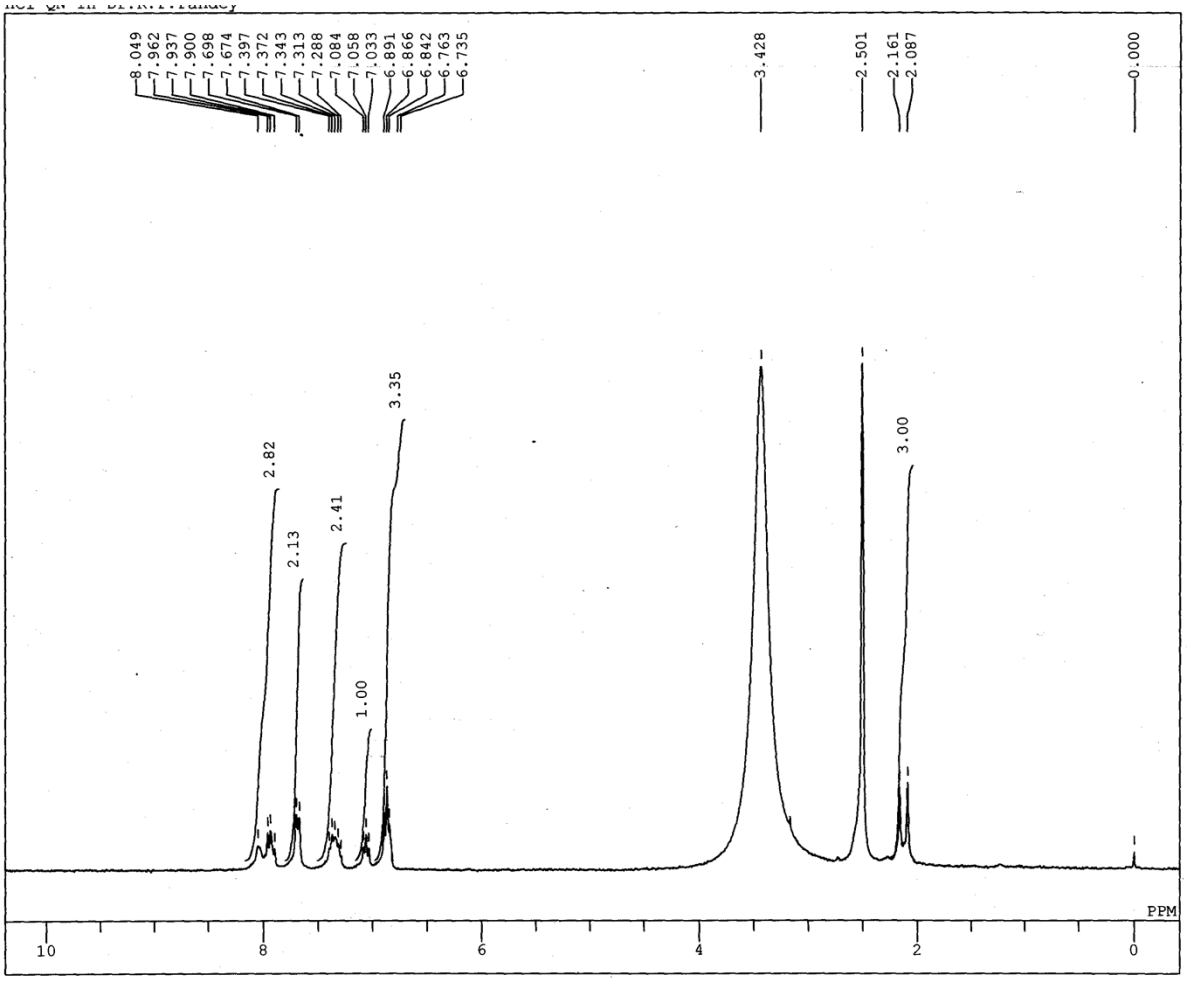

Fig. S4a ^{1}H NMR spectrum of **1**+HCl in dmso-d_6

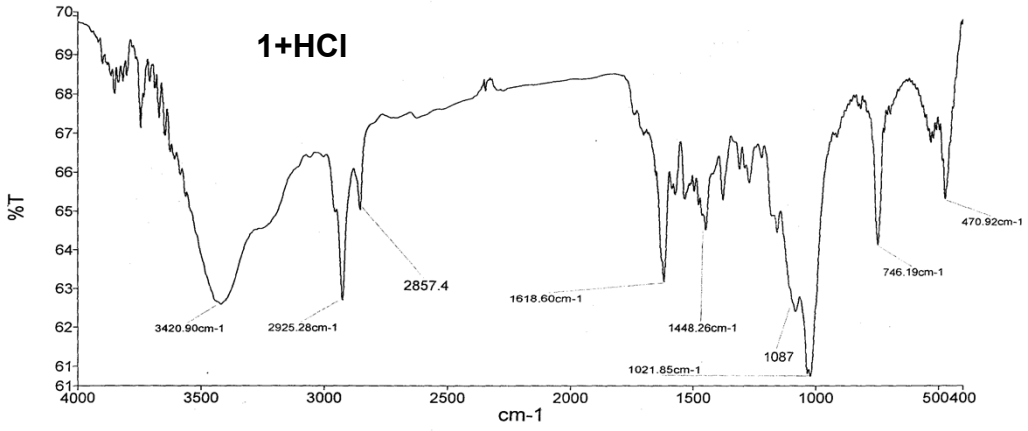

Fig. S4b IR spectrum of **1**+HCl

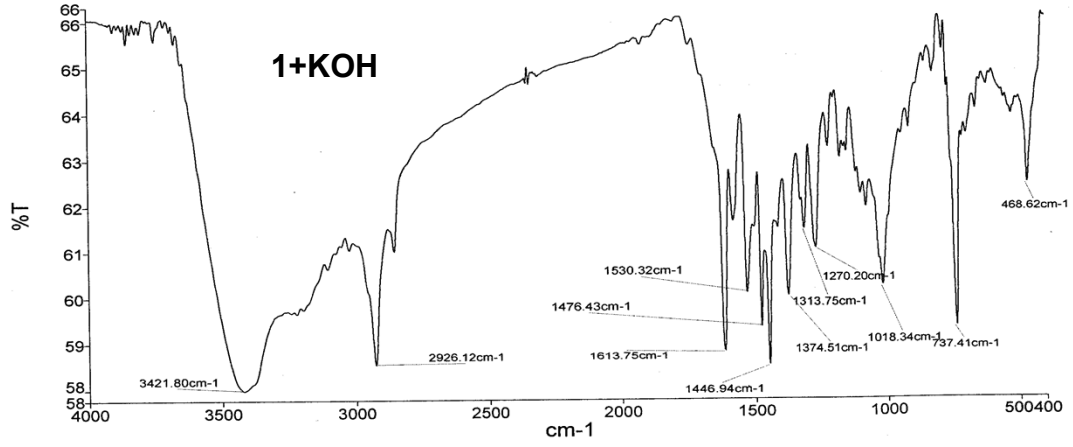

Fig. S4c IR spectrum of **1**+KOH

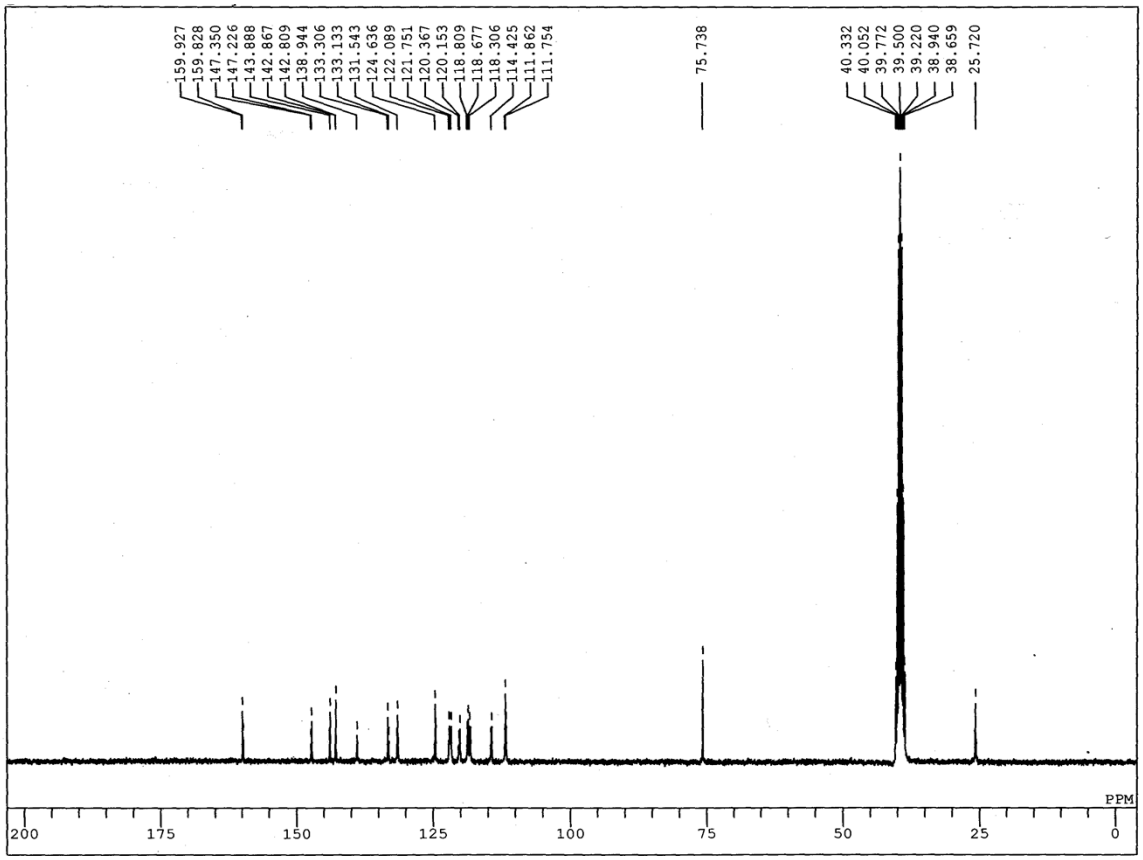
159.927
159.828
147.350
147.226
143.888
142.867
142.809
138.944
133.306
133.133
131.543
124.636
122.089
121.751
120.367
120.153
118.809
118.677
118.306
114.425
111.862
111.754
75.738
40.332
40.052
39.772
39.500
39.220
38.940
38.659
25.720
PPM
200
175
150
125
100
75
50
25
0

S5a

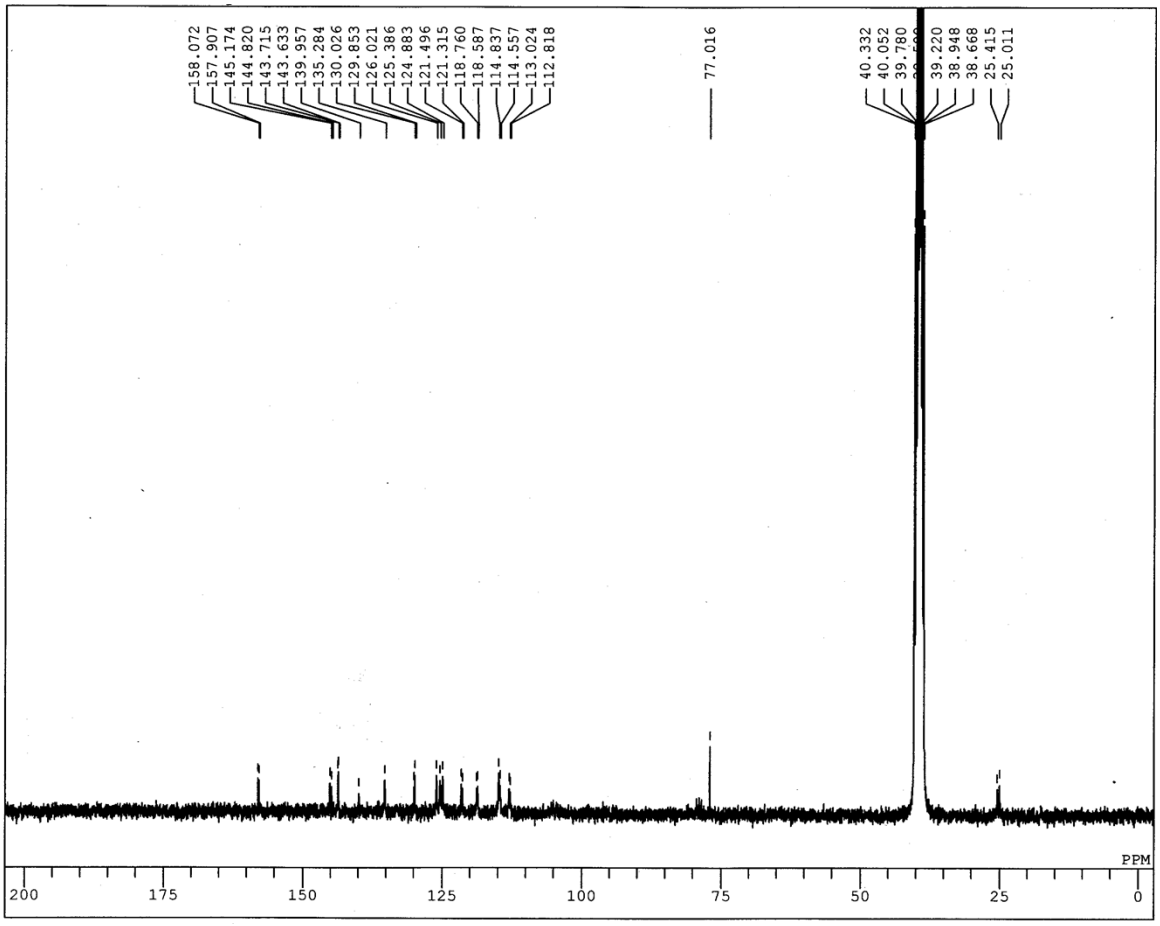

S5b

Fig. S5 ^{13}C NMR spectra of **1** (S5a), and **1'** (S5b) in dmso-d_6

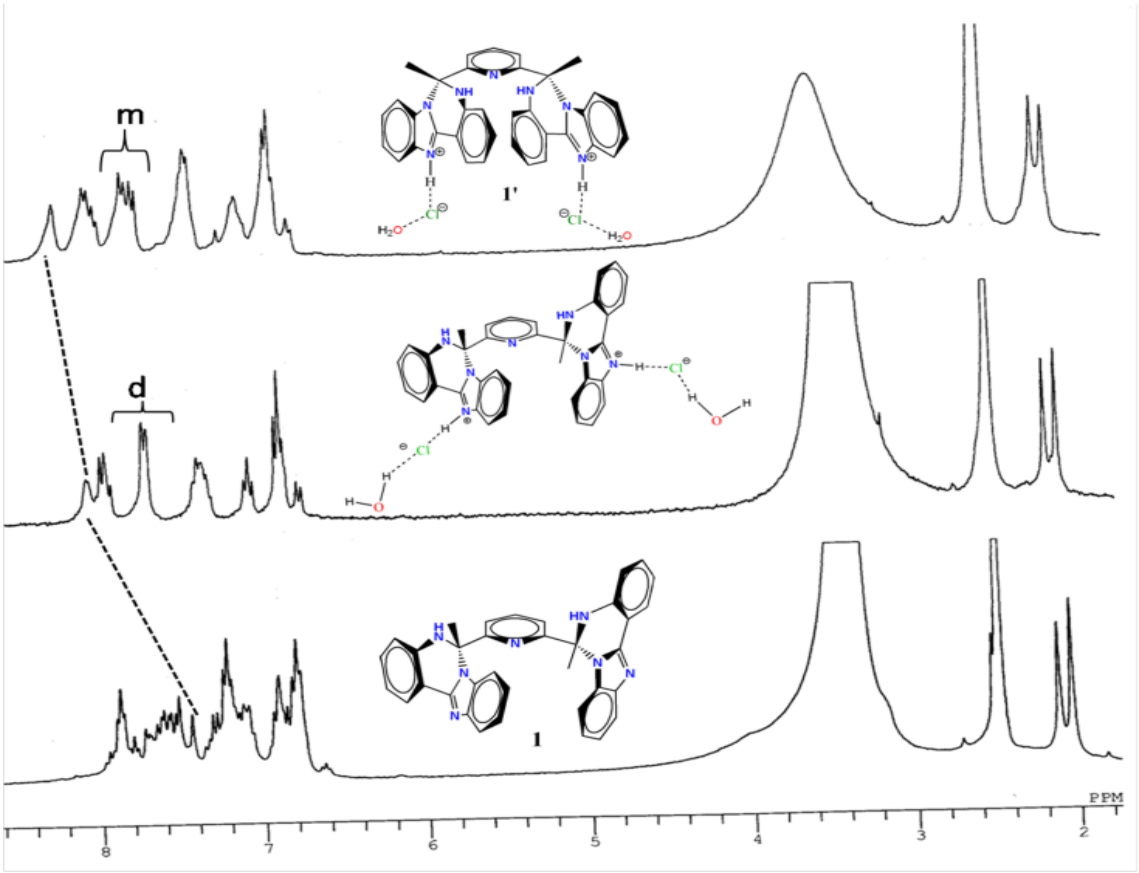

Fig. S6 Stacked ^{1}H NMR spectra of **1**(bottom), **1**+HCl (middle) and **1'** (top) in dmso-d_6.

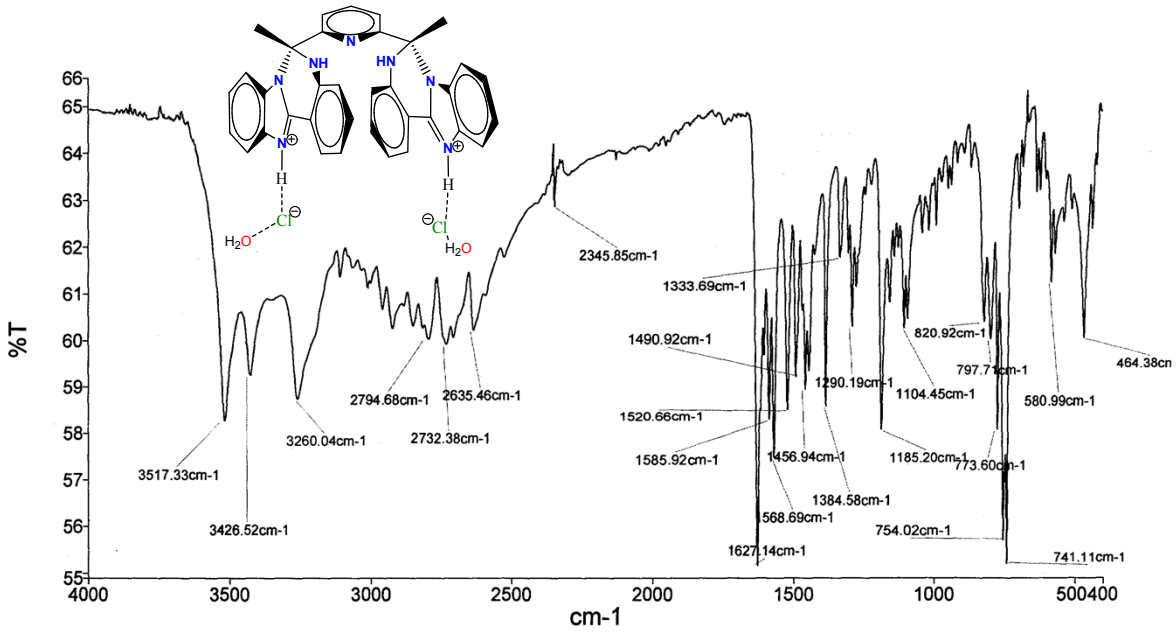

Fig. S7a IR spectrum of **1'**

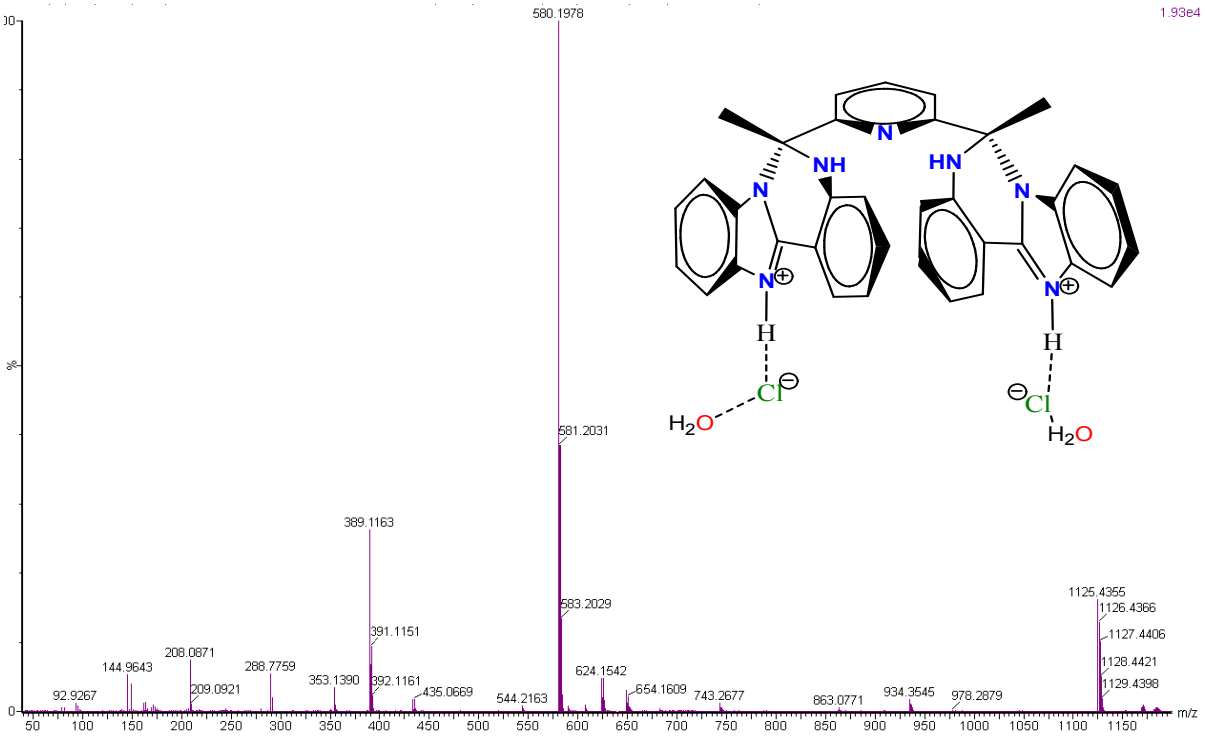

Fig. S7b HRMS spectrum of **1'**

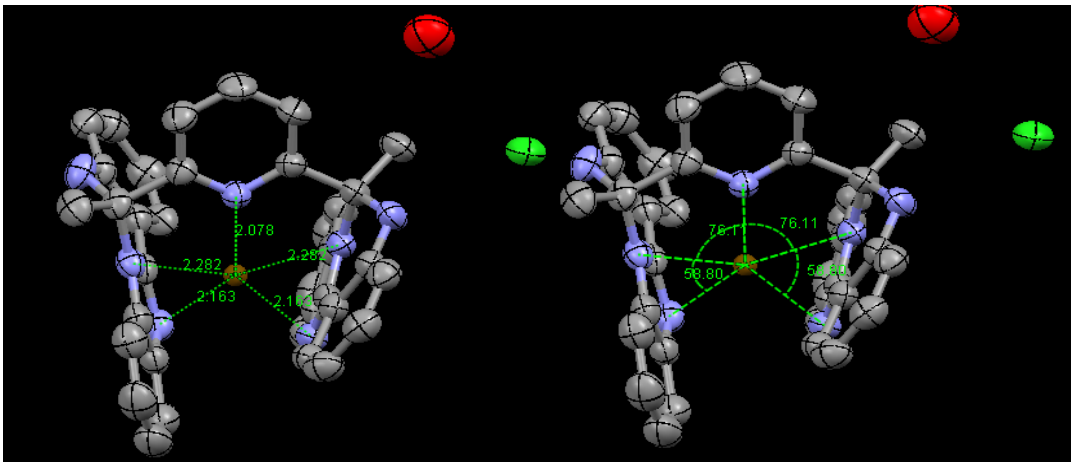

Fig. S8 Calculated bond distances and angles between artificially created centroid and donor sites of **1'**

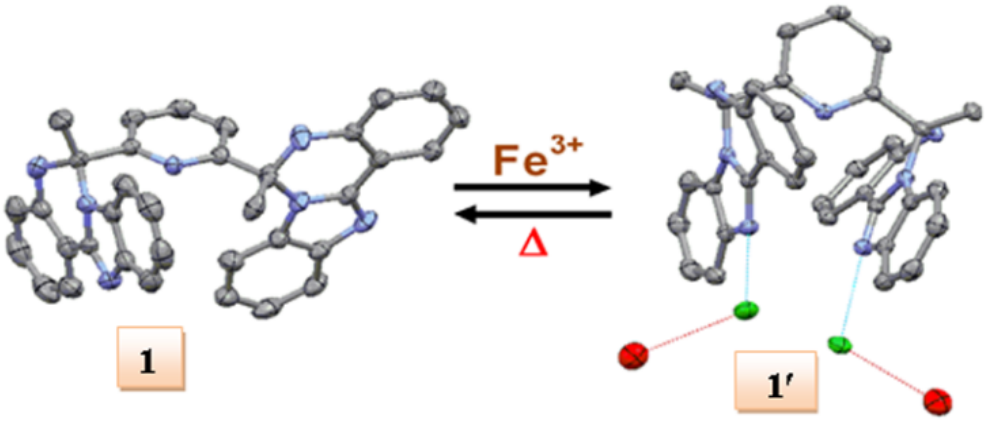

Fig. S9 Crystal structures of **1** (left) and **1'** (right) and their thermoreversible nature.

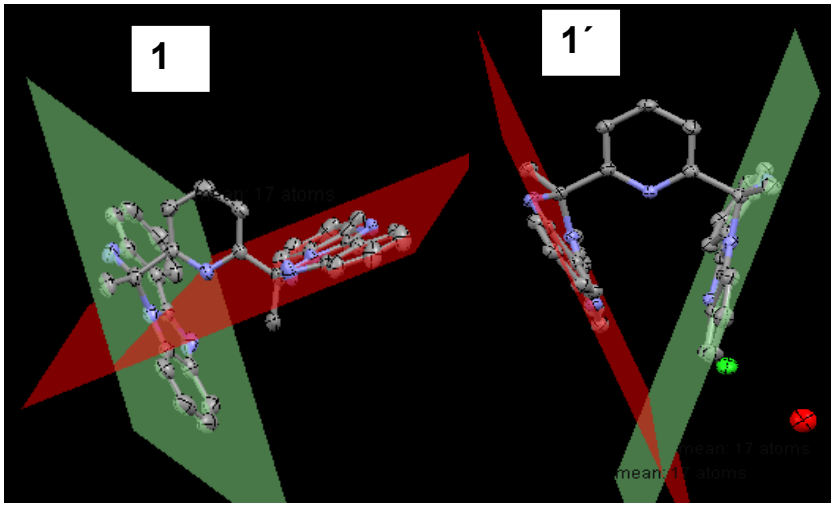

(a)

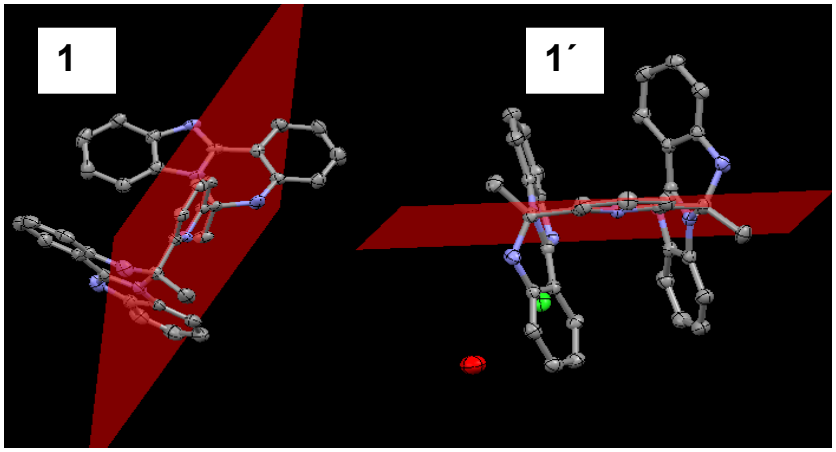

(b)

Fig. S10 Symmetrical comparisons between **1** from **1′** *via* various planes considering IQ arms (a) and central pyridine ring (b)

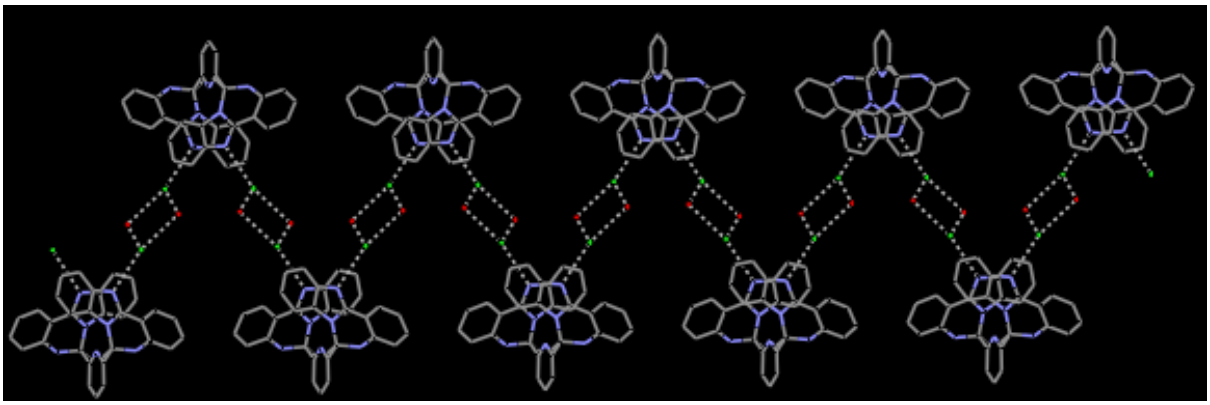

(a)

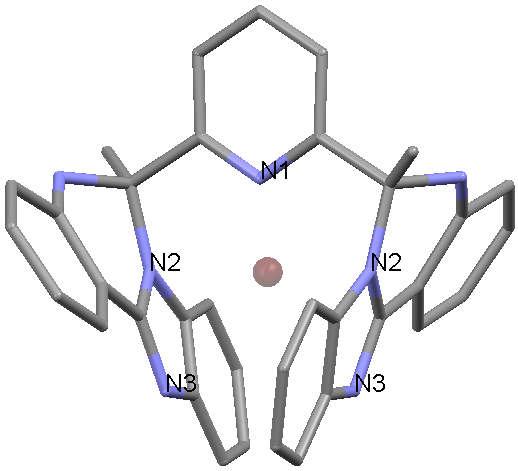

(b)

Fig. S11 (a) Rectangular water-chlorine channels resulting from H···bonding in **1′** (b) An artificially created centroid among donor sites of **1'**

1. ^{1}HNMR description:

It is well documented that solution of $FeCl_3$ in water generates strong acid HCl which could be the driving force for conversion of **1** into **1'**. In this context, ^{1}H NMR spectrum of the compound isolated from reaction between **1** and conc. HCl (~ 3.0 equiv) was also acquired (*p*H ~2.6; Fig. S4a and Fig. S6). The ^{1}H NMR spectrum of this compound displayed –NH (*H*1) protons at δ 8.05 ppm ($\Delta\delta$, 0.61 ppm) while methyl protons resonated as singlet at 2.16 and 2.09 ppm. *H*4 and *H*7 protons resonated at 7.93 ppm ($\Delta\delta$, 0.05 ppm) and *H*9–*H*11 appeared in the range δ 6.73–6.89 ppm (no downfield shift).

2. Crystal structure description

The IQ arms in **1** are almost mutually perpendicular with an interplanar angle of 78.44°, whereas these lie almost parallel in **1'** with an interplanar angle of 41.01° crossing beyond the molecule (Fig. S10a). In **1**, all the members of IQ rings are fairly planar, whereas in **1'** almost half of these lie out of the plane with a deviation of 0.177-0.263 Å. However, deviation of the atoms from plane is similar for both the IQ rings in **1'**. One of the methyl groups in **1** is oriented in the central pyridyl ring plane and other one out of the plane, whereas in **1'** both of these lie out of the pyridyl ring plane (Fig. S10a). Methyl-methyl distance in **1** is 5.533 Å whereas it is 7.235 Å in **1'**. Bite angles about sp^3 hybridized carbon centres are 107.56–113.76° (**1**) and 105.56–112.41° (**1'**) which are very close to ideal T_d geometry that compels the nitrogen atoms to be positioned in a non-chelating fashion both in **1** and **1'**. However, intramolecular N···N distances and their position may be favourable for a metal ion interaction in **1'** (Fig. S8). One of the striking features of **1'** is co-crystallization of two molecules of each of the HCl and H_2O holding its conformation and forming attractive H···bonded Cl(1)···O(1) rectangular channels with distances of 3.219 and 3.257 Å (Fig. S11a). In sharp contrast, only one type of H···bonding interaction involving [N(2)-H(2)···N(4) atoms (2.275 Å)] are present in **1**. It is worth mentioning that **1** involves six C-H···π interactions (2.796-2.889 Å) and lacks completely the π···π interactions, whereas **1'** encompasses edge-to-edge π···π interaction between C(6)···C(8) atoms (3.382 Å) and completely lack any C-H···π interaction. Based on these structural features

it is obvious that **1'** has greater chances to form dimer excited state through face to face interaction.

3. UV/VIS studies

Colorimetric experiments motivated us to scrutinize changes in the absorption of **1** in presence of various metal ions. In its UV/VIS spectrum **1** (Fig. 3a, Main text body) exhibited a low energy (LE) band at 350 nm (ε, 1.56×10^4 $M^{-1}cm^{-1}$) and three high energy (HE) bands at 300 nm (ε, 2.61×10^4 $M^{-1}cm^{-1}$), 290 nm (ε, 2.50×10^4 $M^{-1}cm^{-1}$) and 225 nm (ε, 6.74×10^4 $M^{-1}cm^{-1}$). Addition of the tested metal ions (5.0 equiv; *c*, 100 mM) do not perturb the spectral features for **1**, except Fe^{3+} which leads to a significant hyperchromic and minute red shift (~3-6 nm) in the LE (355 nm, ε, 4.53×10^4 $M^{-1}cm^{-1}$) and HE bands at 306 nm (ε, 5.71×10^4 $M^{-1}cm^{-1}$), 293 nm (ε, 6.23×10^4 $M^{-1}cm^{-1}$) and 225 nm (ε, 12.51×10^4 $M^{-1}cm^{-1}$) (Fig. S12). Notably, these are not the characteristic bands for **1'** because its pure form (isolated from the reaction mixture) displays transitions at 359 nm ($\Delta\lambda$, 09 nm; $\Delta\varepsilon$, 0.38×10^4 $M^{-1}cm^{-1}$), 300 nm ($\Delta\varepsilon$, 1.30×10^4 $M^{-1}cm^{-1}$), 290 ($\Delta\varepsilon$, 1.64×10^4 $M^{-1}cm^{-1}$) and 225 nm ($\Delta\varepsilon$, 3.45×10^4 $M^{-1}cm^{-1}$) (Fig. 3a). The greater optical density for **1**+Fe^{3+}, relative to the isolated pure **1'** may be ascribed to interaction of free metal ion with **1'**.

To gain deep insight into the sensitivity of **1** for Fe^{3+}, titration experiments were carried out under aforesaid conditions. Addition of Fe^{3+} (*c*, 10 mM; 0.0-2.0 equiv) to a solution of **1** leads to incessant hyperchromic shift for both LE and HE bands along with a small red shift (~ 6 nm), and it attains saturation after further additions of Fe^{3+} (Fig. S13). To get an unambiguous mechanism on *p*H or metal triggered conformational changes, **1** was also titrated separately with 1.0 M HCl (~ 3.0 equiv; Fig. S14), which displays significant red shift for the LE band (Δλ, 30 nm) while HE bands shifted hyperchromically (300 nm, $\Delta\varepsilon$, 2.59×10^4 $M^{-1}cm^{-1}$; 290 nm, 3.45×10^4 $M^{-1}cm^{-1}$ and 225 nm, 6.87×104 $M^{-1}cm^{-1}$). It not only suggested protonation of IQ nitrogen, but also conformational retention of **1** as spectral pattern is quite different to that of **1'** and we anticipate this as species (**a**) in Scheme S2. Further, to verify this effect, *p*H of solution containing pure **1'** (isolated from reaction mixture) was also measured and found to be ~3.4. Thus the UV/VIS spectra of **1'** was compared with that of **1** at *p*H ~3.4 and found significantly different (Fig. S15). It further implied inevitability of the Fe^{3+} in the conversion of **1** into **1´**.

4. Photoluminescence studies

To gain deep insight into the role of *p*H on conformational switching, an alternative titration experiment between **1** and Fe^{3+} was carried out using methanol as the sole solvent. The obtained results were significantly different to what were observed using H_2O-MeOH (8:2) media (Fig. S21). It was observed that results are quite different relative to that obtained using H_2O-MeOH (8:2) media. Addition of Fe^{3+} (0.2-0.6 equiv) causes small PL quenching (55%) and very small red shift (Δλ, ~10 nm), whereas increasing the concentration of Fe^{3+} (0.8 equiv) leads to a considerable red shift (λ_{em}, 460 nm, dotted blue line, *p*H ~6.6; Fig. S21), and this species may be considered as intermediate between **1** and **1′**. The addition of higher concentrations of Fe^{3+} (0.9-2.0 equiv) induces rapid red shift (480 nm, Δλ ~50 nm, *p*H ~4.8). **The *p*H of 1+Fe^{3+} (2.0 equiv) solution in H_2O-MeOH and pure MeOH were different, and the results indicated greater PL quenching in H_2O-MeOH (*p*H ~3.4) relative to methanol (*p*H ~4.8).** On the other hand, titration of **1** with 1.0 M HCl (~3.0 equiv, Fig S22) led to a large PL quenching (~90%) with relatively small red shift (Δλ, ~33 nm; λ_{em}, 460 nm) that differs from characteristic emission of **1'** (λ_{em}, 480 nm, $\Delta\lambda_{em}$, ~53 nm; 44% '*turn-on*'). Thus, it can be concluded that conformational switching of **1** to **1'** is selectively triggered by Fe^{3+}.

Moreover, $Fe(NO_3)_3 \cdot H_2O$ (another Fe^{3+} salt) was also used as alternative iron source which exhibited results similar to that for $FeCl_3$. Overall studies enabled us to conclude that addition of Fe^{3+} primarily protonates the nitrogen of IQ arms in **1** followed by Fe^{3+} triggered conformational transformation.

5. Theoretical Studies

Density Functional Theory (DFT) calculations have been performed regarding said assumptions, and found the distribution of electron densities on the highest occupied molecular orbital (HOMO) and lowest unoccupied molecular orbital (LUMO) perturbed for **1'** compared to **1** (Fig. S24, Fig. S25; Table S3). LUMO in both cases is mainly located on the central pyridine core and HOMO on one of the IQ arms in **1**, whereas it is localized largely on one chloride and to a lesser extent on closest phenyl ring of the opposite arm along with one of the two oxygen atoms in **1'** (Fig. S24). The already discussed single exponential decay of **1** in methanol (τ, 8.7 ns) is considered to be rather long compared to common fluorescent emitters (Fig. S19). This

suggests that an internal charge transfer (ICT) between pyridine core and other part of the molecule is responsible for de-excitation mechanism or because of the restricted molecular movement by already mentioned stabilization effect through hydrogen bonding.[16]

6. Thermal studies

Further, reversibility in a conformational rotary is as important as controlling and isolation of the conformers, therefore, solution of **1'** was heated at 5 °C/min from 27- 80°C (Fig. S26). Notably, changes were observed in fairly opposite direction and **1** almost completely regenerated at 80 °C. Remarkably, PL quenching in the reverse spectra was only 32% owing to evaporation of H···bonded HCl at higher temperatures, consequently *p*H of the solution rises toward neutral to afford **1**.

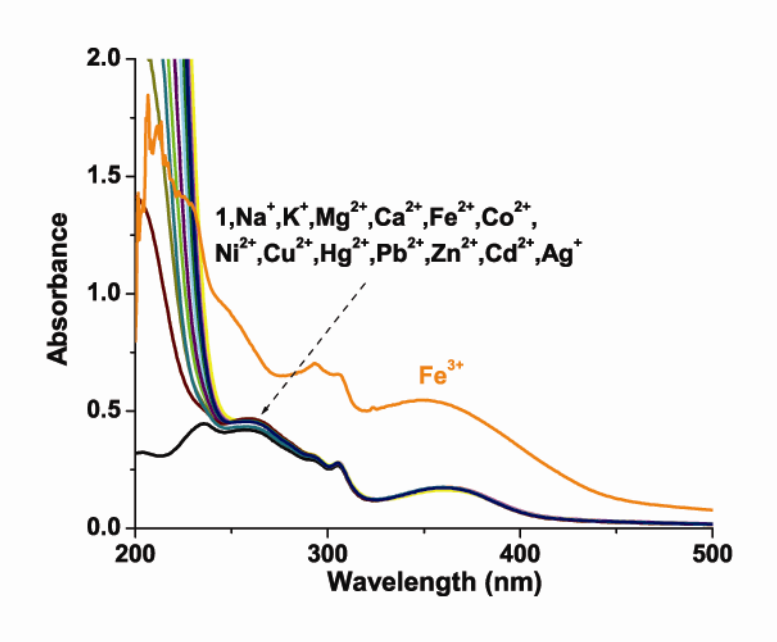

Fig. S12 UV/VIS spectra of **1** in presence of 5.0 equiv of various metal ions (*c*, 100 mM)

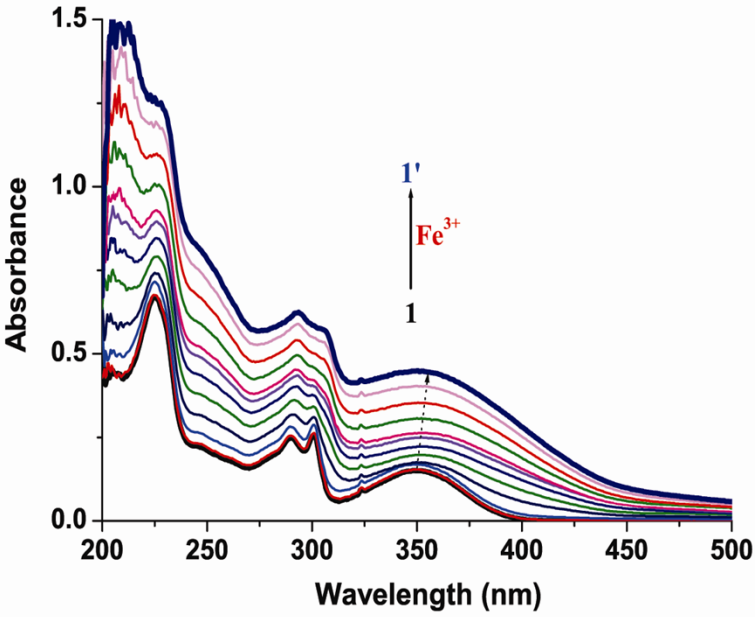

Fig. S13 UV/VIS titration plot for **1** (*c*, 10 μM) in various aliquots of Fe^{3+} (0.0-2.0 equiv; *c*, 10 mM)

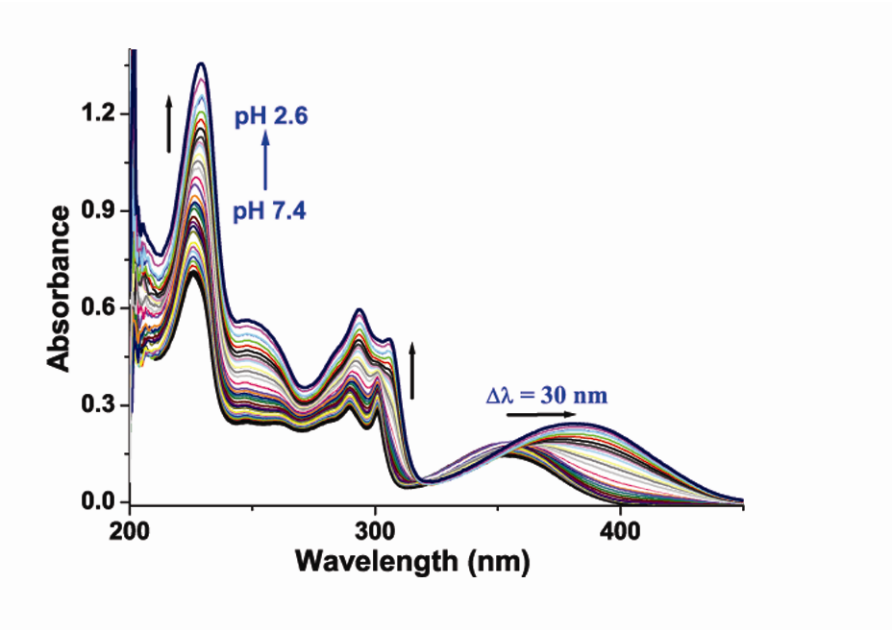

Fig. S14 UV/VIS titration plot for **1** (*c*, 10 μM) with 1.0 M HCl solution

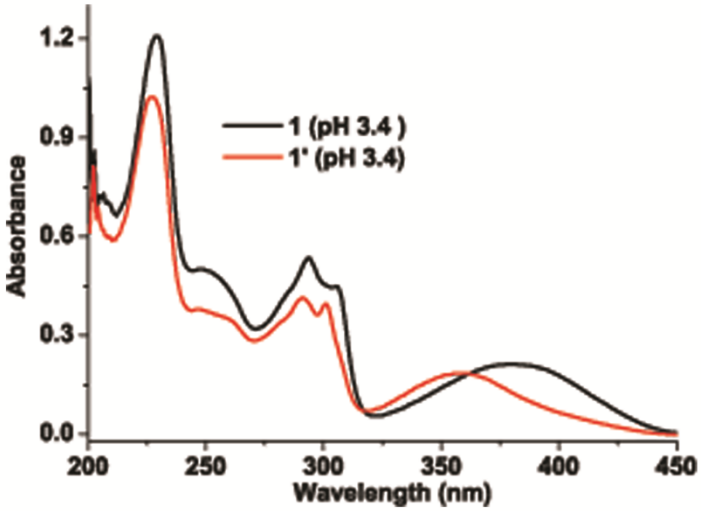

Fig. S15 UV/ VIS spectra for **1** and **1′** at *p*H 3.4 (*c*, 10 μM)

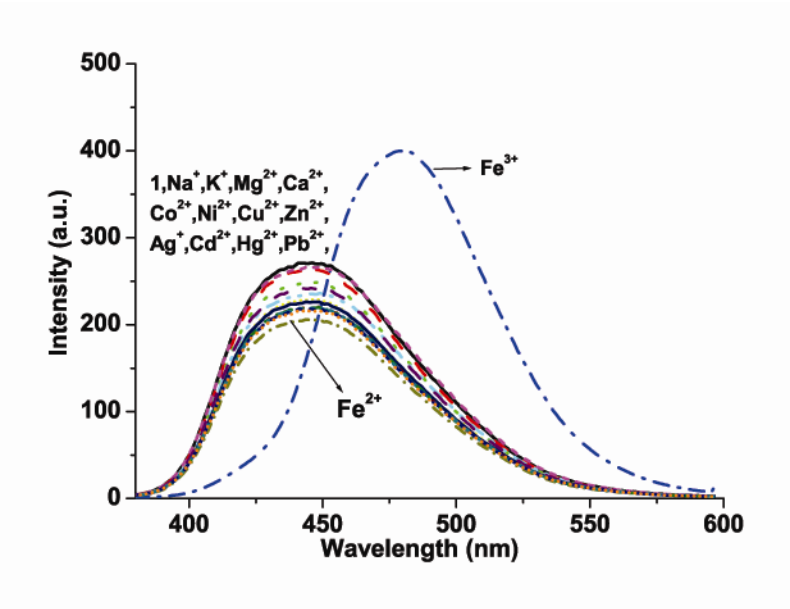

Fig. S16 Photoluminescence (PL) spectra of **1** in presence of 5.0 equiv of various metal ions (*c*, 100 mM)

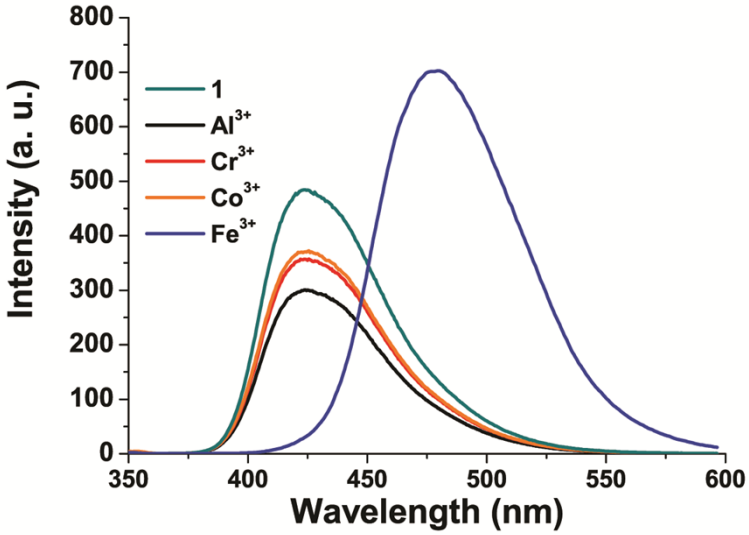

Fig. S17 PL spectra of **1** (*c*, 10 μM) in presence of 5.0 equiv of various metal (III) ions (*c*, 100 mM)

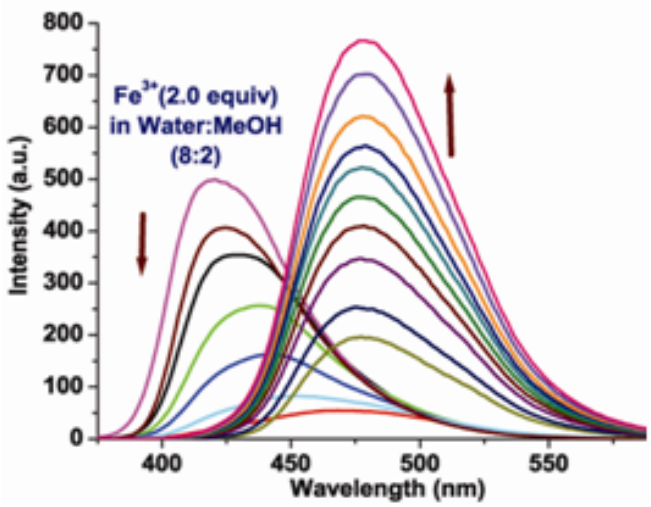

Fig. S18 Fluorescence plot titrated between **1** and Fe^{3+} (0.0-2.0 equiv) to produce **1'**

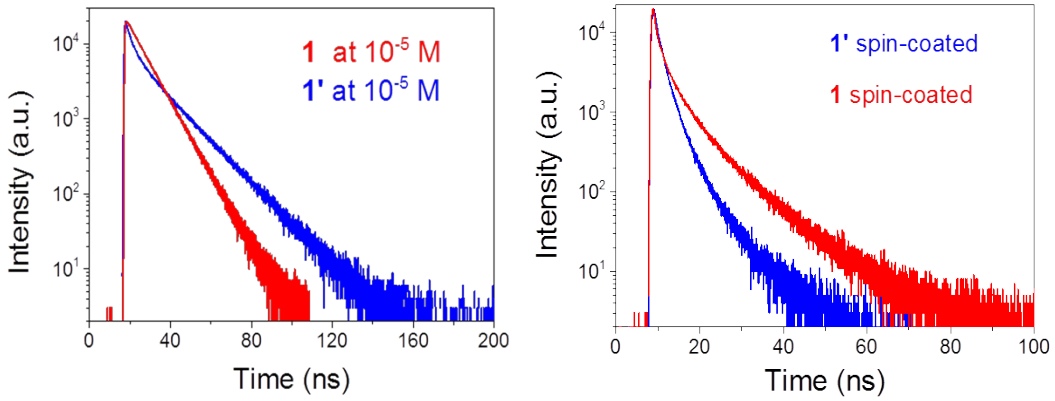

Fig. S19 Transient photoluminescence decay of **1** and **1′** in powder (left) and spin coated films (right).

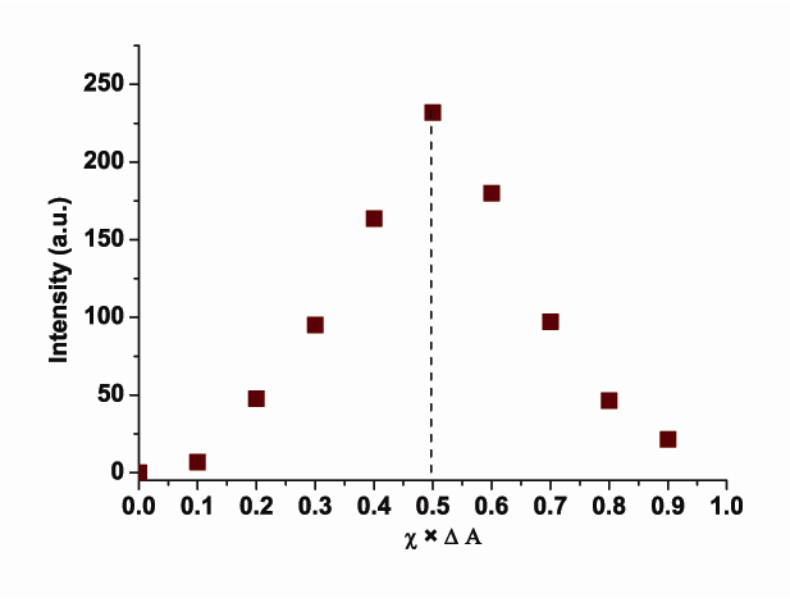

Fig. S20 Job's plot showing 1: 1 stoichiometry between **1** and Fe^{3+}

.

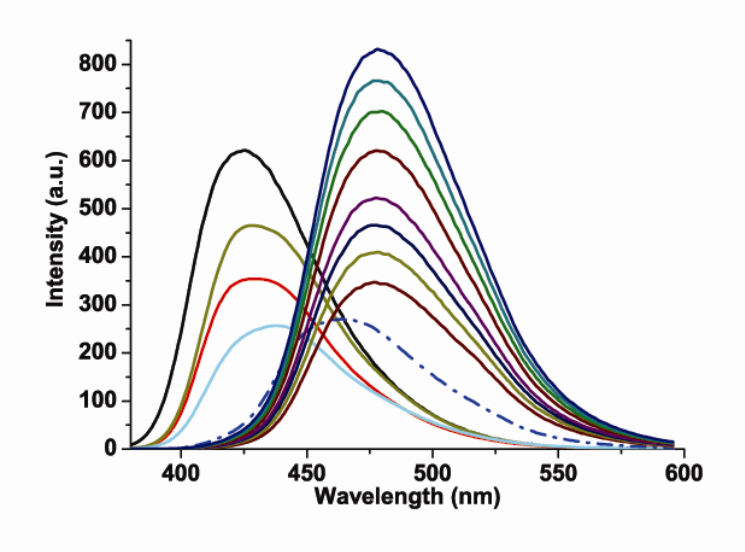

Fig. S21 PL titration plot for **1** (*c*, 10 μM in MeOH) in presence of Fe^{3+}

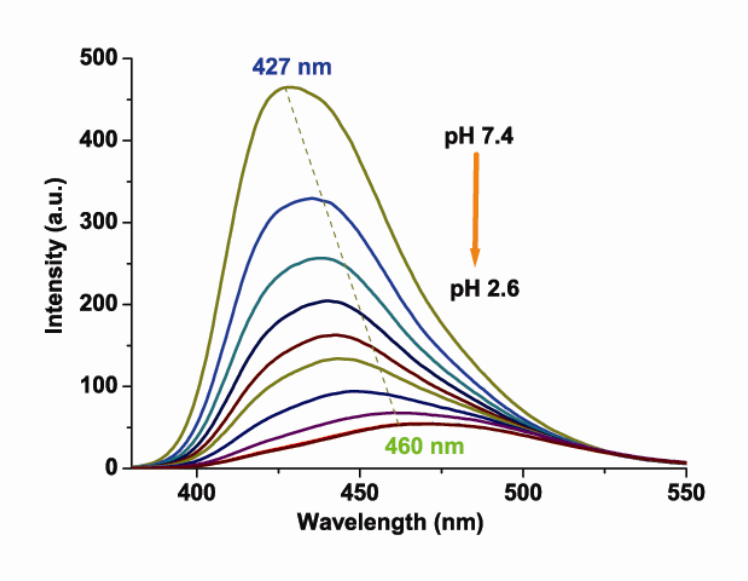

Fig. S22 PL titration plot for **1** (*c*, 10 μM) with 1.0 M HCl

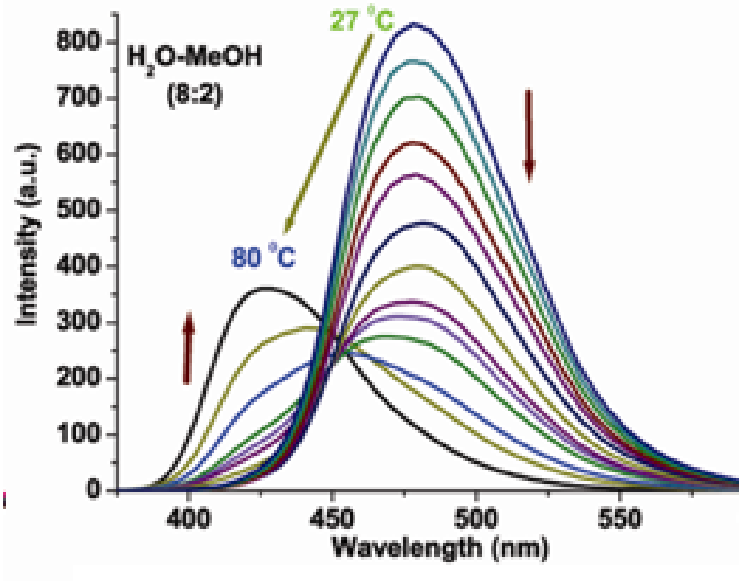

Fig. S23 Thermo-reversibility plot for conversion of **1'** to **1** upon heating the solution

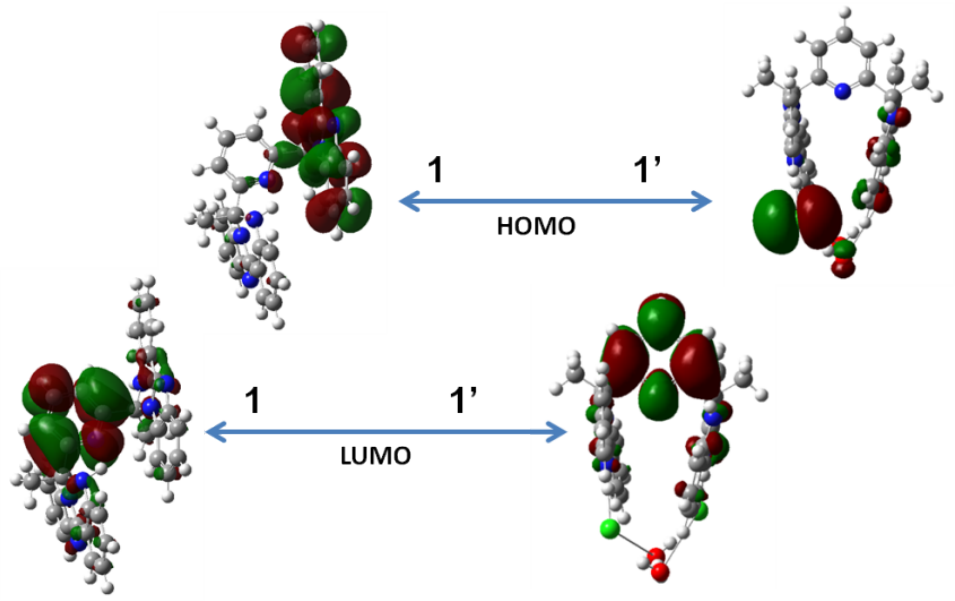

Fig. S24 Distributions of electron densities in the HOMO and LUMO states of **1** and **1′**.

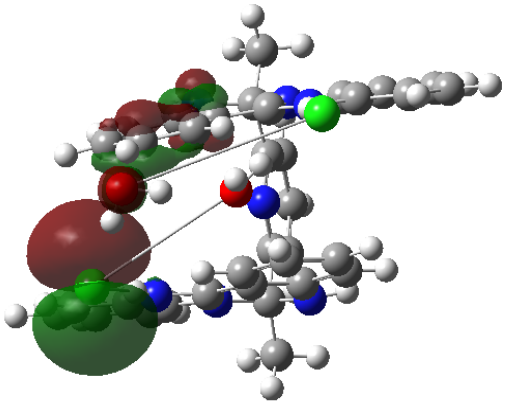

Fig. S25 Distribution of electron density in the HOMO state of **1′** calculated by DFT in Gaussian 09 at the B3LYP/6-31G(d) level

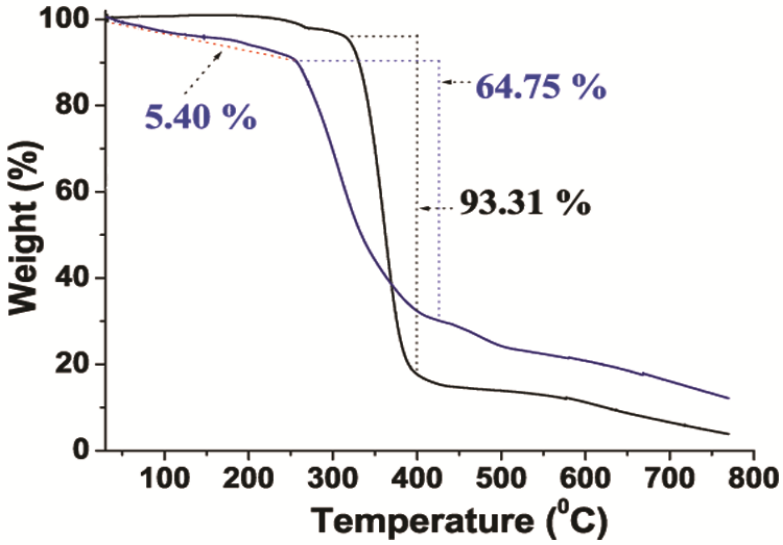

Fig. S26 TGA pattern (d) of **1** (black line) and **1′** (Blue line).

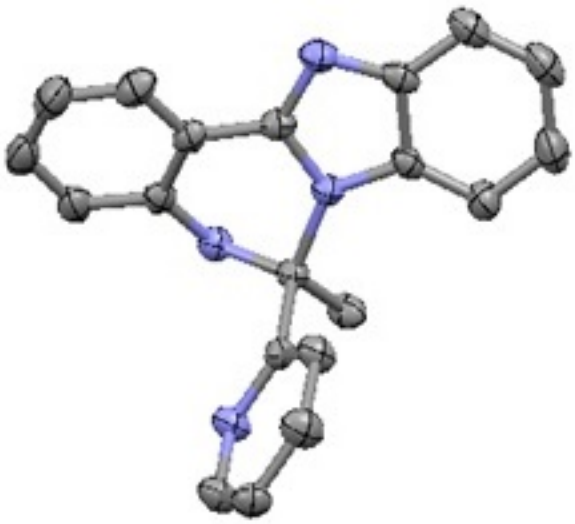

Fig. S27 Crystal structure of model compound **M**

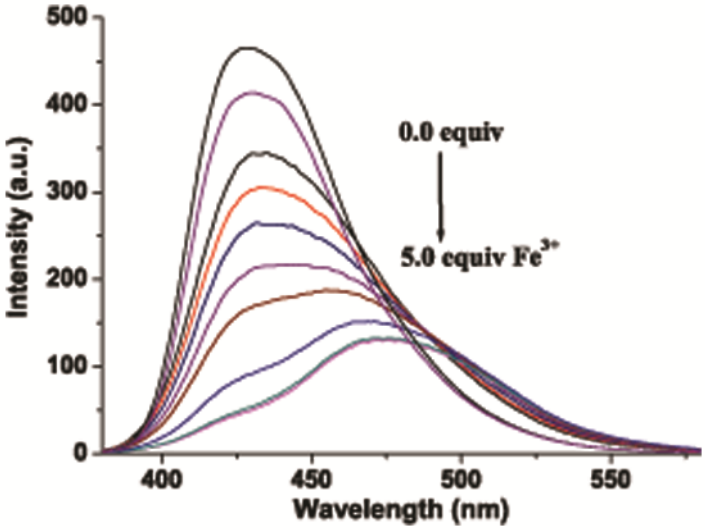

Fig. S28 Fluorescence response of model compound **M** toward Fe^{3+}

Table S1. Comparative ^1H NMR data for **1**, **1´** and **1**+HCl

1	**1+HCl**	**1´**
δ(ppm)	**δ(ppm)**	**δ(ppm)**
7.88 (d)	8.04 (s, *br*)	8.20 (s, *br*)
7.62-7.52 (m)	7.93 (t)	8.02-7.96 (m)
7.44 (s)	7.68 (d)	7.79-7.70 (m)
7.32-7.13 (m)	7.40-7.29 (m)	7.38 (m)
6.91-6.80	7.06 (t)	7.08 (s)
(m)	6.87 (t)	6.88 (d)
2.12 (s)	6.75 (d)	2.18 (s)
2.05 (s)	2.16 (s)	2.11 (s)
	2.09 (s)	

Table S2. Crystallographic refinement parameters for **1, 1'** and **M.**

Crystal data	**1**	**1'**	**M**
Empirical formula	$C_{35}H_{27}N_7$	$C_{35}H_{27}Cl_2N_7O_2$	$C_{20}H_{16}N_4$
Crystal system	Monoclinic	Monoclinic	Monoclinic
Space group	*P2₁/n*	*C2/c*	*P2₁/n*
a (Å)	11.98(3)	15.79(7)	6.86(3)
b (Å)	19.84(5)	11.54(4)	12.80(6)
C (Å)	12.53(3)	17.13(7)	18.24(8)
α	90.00	90.00	90.00
β	112.80(2)	99.28(4)	91.86(3)
γ (°)	90.00	90.00	90.00
V (Å^3)	2744.9(1)	3083.1(2)	1601.3(1)
Z	4	4	4
F(000)	1144	1368	656
ρ_{calc} (Mg m^{-3})	1.320	1.410	1.296
M (g mol^{-1})	545.64	654.58	312.37
T (K)	293(2)	293(2)	153(2)
μ (mm^{-1})	0.081	2.266	0.080
refln collected	34823	5566	29966
parameters refined	379	226	219
GOF on F^2	1.016	1.023	1.030
final R1 on observed data	0.0765	0.0450	0.0518
final wR2 on observed data	0.2273	0.1240	0.1363

Table S3. Calculated photophysical properties of **1** and **1′ - DFT, Gaussian 09, B3LYP/6-31G(d)**

Molecule	HOMO [eV]	LUMO [eV]	S_1[(a)] [eV, nm]	T_1[(b)] [eV, nm]	μ [D]	μ^* [D]
1	-5.46	-1.48	3.35, 370	2.79, 445	4.90	13.10
1'	-5.39	-2.33	2.65, 468	2.51, 494	25.19	10.26

Table S4. PL data of **1** and **1'** in methanol, film and powder

Compound	Φ [%]	$\lambda_{em\text{-}peak}$, $\lambda_{em\text{-}onset}$ [nm]	$\lambda_{ab\text{-}peak}$[a], $\lambda_{ab\text{-}onset}$ [nm]	τ_1, τ_2 [ns]	A_1[b], A_2	Decay1, Decay2[c] [%]
1 (solution)	100	427, 394	350, 400	8.7	20809	100
1′(solution)	72.4	480, 406	359, 441	3.03, 15.13	11669, 8338	21.9, 78.1
1(film)	24.0	461, 408	358, 401	1.33, 7.04	15941, 3775	44.4, 55.6
1'(film)	25.0	480, 428	375, 452	1.48, 4.44	18737, 2657	70.2, 29.8
1(powder)	21.9	443, 417	-	-	-	-
1'(powder)	26.2	476, 438	-	-	-	-

References:

1. D.D. Perrin, W. L. F. Armango, D. R. Perrin, Purification of laboratory Chemicals, Pergamon: Oxford, U.K. 1986.

2. G. M. Sheldrick, *SHELXL-97, Program for X-ray Crystal Structure Refinement*; Gottingen University: Gottingen, Germany, 1997; G. M. Sheldrick, *SHELXS-97, Program for X-ray Crystal Structure Solution*; Gottingen University: Gottingen, Germany, 199**7**.

3. A. L. Spek, *PLATON, A Multipurpose Crystallographic Tools* Utrecht University, Utrecht, The Netherlands, 2000; A. L. Spek, *Acta Crystallogr. A* 1990, **46**, C31.